

Synthesis of ZrO₂ nanoparticles in microwave hydrolysis of Zr (IV) salt solutions—Ionic conductivity of PVdF-co-HFP-based polymer electrolyte by the inclusion of ZrO₂ nanoparticles

N.T. Kalyana Sundaram, T. Vasudevan, A. Subramania*

Advanced Materials Research Lab, Department of Industrial Chemistry Alagappa University, Karaikudi 630 003, India

Received 6 June 2006; received in revised form 16 October 2006; accepted 10 November 2006

Abstract

Nanocrystalline ZrO₂ particles have been prepared by microwave hydrolysis of Zr(IV) salt solutions at 400 °C for 6 h. The paper describes the PVdF-co-HFP-ZrO₂-based NCPs prepared by a simple solvent casting technique. The incorporation of ZrO₂ nanoparticles in the PVdF-co-HFP matrix, improved the ionic conductivity due to the availability of a large amount of oxygen vacancies on ZrO₂ surface which may act as the active Lewis acidic site that interact with ClO₄⁻ ions. On the other hand, a high concentration of ZrO₂ [10 wt(%)] leads to depression in ionic conductivity due to the formation of more crystalline phase in the PVdF-co-HFP matrix. DSC, XRD, SEM and DC-polarization studies were carried out. This paper also explores and proposes a structure–conductivity correlation in the PVdF-co-HFP-LiClO₄–ZrO₂-based NCPs system. The proposed correlation is derived from the interpretation of DSC, XRD and AC-impedance measurements. The temperature dependence of the ionic conductivity of NCPs follows the Arrhenius behaviour. Finally, the LSV experiment has been carried out to investigate the electrochemical stability in the polymer electrolytes.

© 2006 Published by Elsevier Ltd.

Keywords: A. Polymer; A. Thin film; C. Differential scanning calorimetry; D. Transport properties

1. Introduction

The development of a new polymeric system to be used as an electrolyte in advanced batteries and fuel cells is critical for the commercial success of these types of power systems [1]. Because these polymer electrolytes often show insufficient conductivity, poor mechanical stability and decrease in interfacial stability. Consistent research efforts have been devoted to increase the ionic conductivity and to lower the operation temperature of the polymer electrolyte to near ambient temperature [2]. The addition of liquid solvent is one of the approaches. However, this promotes deterioration of mechanical properties of the polymer electrolyte and increases its reactivity towards the electrodes. Generally, various methods have been applied to reduce the crystallinity of the polymer electrolytes while maintaining their flexibility and mechanical stability which

extends over a wide temperature range. Among them, the addition of inert materials into polymer electrolyte has attracted considerable attention due to its improved mechanical stability, enhanced ionic conductivity, lithium transference number, electrolyte–electrode interfacial stability, etc. [3–7]. Scrosati et al. [8] reported that an improvement in the cationic transference number and the interfacial stability between the polymer electrolyte and lithium metal electrode were achieved by the addition of ceramic fillers such as SiO₂, TiO₂, γLiAlO₂, etc. Further, MgO, CaO, CuO, etc., have also been tried which have positive free energy of lithium and should avoid the formation of dendrites growth and passivation of metallic lithium at the electrode–electrolyte interface and also enhance the conductivity of the polymer electrolyte which depends upon the particle size and annealing temperature [9–13].

The micro-size ceramic oxides will increase the large degree of preferential orientation in polymer electrolyte film, which leads to non-conducting planes being

*Corresponding author.

E-mail address: drasubramania@yahoo.co.in (A. Subramania).

perpendicular to the current path and thus reduces the conductivity [14]. To avoid this problem, in the present investigation, ZrO₂ nanoparticles were synthesized and used for the preparation of NCPM using poly(vinylidene fluoride-co-hexafluoropropylene) PVdF-co-HFP as the polymer matrix. Finally, the DSC, XRD, SEM, AC-impedance spectroscopy and DC-polarization studies were also investigated.

2. Experimental

The ZrO₂ nanoparticles were synthesized by the hydrolysis of Zr(IV) salts in aqueous–alcohol solution. An initial aqueous–alcohol solution was prepared from distilled water and tert butyl alcohol. This solution was mixed with aqueous solutions of zirconyl salts ZrO(NO₃)₂ in ratios such that the zirconium concentration was 0.128 M and the alcohol-to-water ratio was 5:1. The initial solution in a glass flask was placed in a micro-wave oven (input power 300 W). The solution was heated to the boiling point (3–5 min) and the oven was switched off. Then the solution was neutralized with 20% ammonia solution, which prevented the precipitate formed in the course of micro-wave hydrolysis from being dissolved on cooling. This precipitate was centrifuged (4000 rpm, 10 min), washed with distilled water until the reaction towards NO₃⁻ was negative, dried at 60 °C for 3 h and annealed at 400 °C for 6 h. The phase purity and the degree of crystallinity of the resulting ZrO₂ sample were monitored by XRD analysis. Surface morphology of ZrO₂ nano-particle was measured by scanning electron microscopy on a JOEL JSM-35CF microscope.

PVdF-co-HFP with an average molecular weight greater than 5,00,000 (Aldrich, USA) and LiClO₄ (E-Merck, Germany) were dried in vacuum oven at 50 °C under 10⁻³ torr pressure for 48 h. EC&DEC (Across organic, Belgium) were purified by distillation under reduced pressure.

The PVdF-co-HFP-ZrO₂-based nano-composite polymer electrolyte membranes (NCPMs) were made by a simple solvent casting technique. The solution of PVdF-co-HFP in AR grade acetone was prepared in which ZrO₂ nanoparticles was dispersed and sonicated. After sonication, a homogeneous colloidal solution was obtained which was cast and dried into a film form of about 50–80 μm thickness. The amount of inclusion of ZrO₂ nanoparticles used in the polymer matrix is 2–10 wt(%) to prepare nano-composite polymer membranes (NCPMs). Finally, the NCPMs were soaked in 1 M LiClO₄ containing (1:1 (v/v)) ratio of EC-DEC for 18 h to get NCPMs.

Thermal behaviour of the NCPMs was studied by using a differential scanning calorimeter (Dupont TA-2000 DSC). Each sample was scanned from 0 to 200 °C by heating at a scan rate of 10 °C/min under N₂ atmosphere. The crystallinity of the NCPMs were calculated using Eq. (1) from the DSC curves [15],

$$X_c(\%) = (\Delta H_m / \Delta H_m^\phi) \times 100, \quad (1)$$

where, ΔH_m^ϕ is the crystalline melting heat of pure PVdF (104.7 J/g), ΔH_m is the heat of fusion of PVdF-co-HFP-ZrO₂-based NCPMs. It can be calculated from the integral area of the baseline and each melting curve.

The X-ray diffraction (XRD) patterns were recorded with JOEL (JDX-8030) diffractometer using nickel filtered Cu–K α radiation at a scan rate of 10 °C/min to examine the nature of crystallinity with respect to ZrO₂ nanoparticles in the PVdF-co-HFP polymer network. The surface morphology of NCPMs was studied by Scanning electron microscope (JOEL JSM-35CF).

The ionic conductivity measurements were performed by sandwiching the NCPM in between two stainless steel electrodes using HIOKI 3522-50 LCR meter over a frequency range of 1 mHz–100 kHz at a scan rate of 1 mV/s with various temperatures ranging from 298 to 353 K. DC polarization cell was constructed by sandwiching the polymer electrolyte in between the symmetrical lithium metal electrodes and the experiment was performed as described earlier [16] to find out the lithium transference number of NCPMs. The electrochemical stability of polymer electrolyte was studied at room temperature by running a linear sweep voltammetry (LSV) using a two electrode cell in the configuration of Li/ polymer electrolyte /SS at a scan rate of 1 mV/s where lithium acts as a counter and reference electrodes and SS act as a working electrode, respectively. The cell was assembled in a dry box under argon atmosphere.

3. Results and discussion

3.1. XRD and SEM analysis of ZrO₂ nano-particles

The XRD pattern for the synthesized ZrO₂ nanoparticles is shown in Fig. 1. The diffractogram reveals the formation of highly crystalline product with high phase purity on

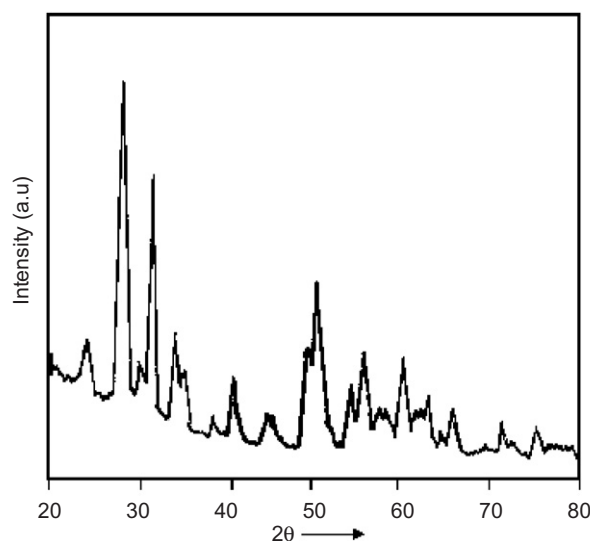


Fig. 1. XRD pattern of ZrO₂ nanoparticles.

calcination at 400 °C for 6 h. The pattern is very similar to that reported for ZrO₂ [17]. The average coherent-scattering domains (CSD) size was calculated by means of the well-known Debye–Scherer formula [18] is 60 nm. Fig. 2 shows the SEM photograph of ZrO₂ nanoparticles. From this figure, the grain size of the particle is found to be ~62 nm with uniform distribution. The value of 62 nm observed from SEM result was in good agreement with the XRD result of 60 nm. It reveals that the microwave hydrolysis makes it possible to obtain particles of predominantly spherical shape, with a narrower size distribution.

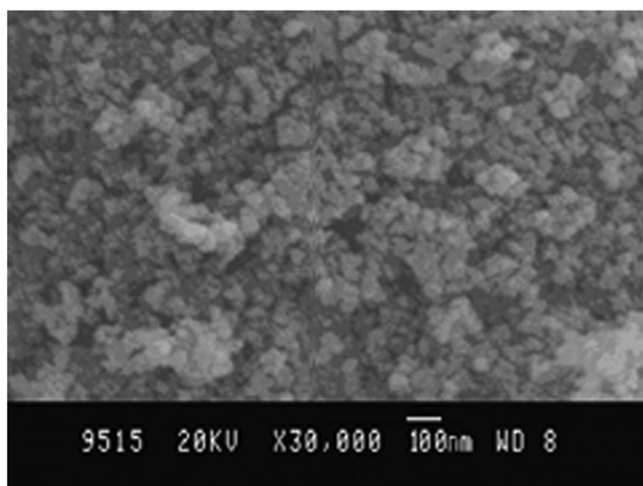


Fig. 2. SEM photograph of ZrO₂ nanoparticles.

3.2. DSC analysis of NCPMs

Fig. 3 (a)–(f) shows the DSC curves of PVdF-co-HFP-ZrO₂-based NCPMs with different wt (%) of ZrO₂ nano-particles [0, 2, 4, 6, 8 and 10 wt (%)] in polymer matrix. From these curves it was observed that the amount of ZrO₂ nano-particles slightly influences the crystalline melting temperature (T_m), heat of fusion (ΔH_m) and crystallinity (X_c) as shown in Figs. 3 and 4. From these figures, it may be seen that the reorganization of polymer chain may be hindered by the cross-linking centres formed by the interaction of the Lewis acid group ceramics with the polar group polymers [19]. The incorporation of ZrO₂ nano-particles, far more compared to the segmental chain motion of the polymer, stabilizes the amorphous structure and thus enhances the ionic conductivity of polymer electrolyte [20]. It can be observed from Figs. 3 and 4 that the T_m , ΔH_m and X_c decreases with increase in ZrO₂ content upto 8 wt(%) to the PVdF-co-HFP system and was found to be 144.4 °C, 82.5 J/g and 76.8%, respectively. Beyond this concentration [10 wt(%) of ZrO₂], T_m , ΔH_m and X_c increases. It may be explained by the assumption that immobilization of PVdF-co-HFP polymer chain segments due to the steric hindrance caused by both PVdF-co-HFP and ZrO₂ nano-particles will induce crystalline site in the polymer matrix which leads to lower segmental mobility. Hence, 8 wt (%) of ZrO₂ nanoparticles incorporated in PVdF-co-HFP matrix has been taken as an optimized composition for lithium-ion battery applications.

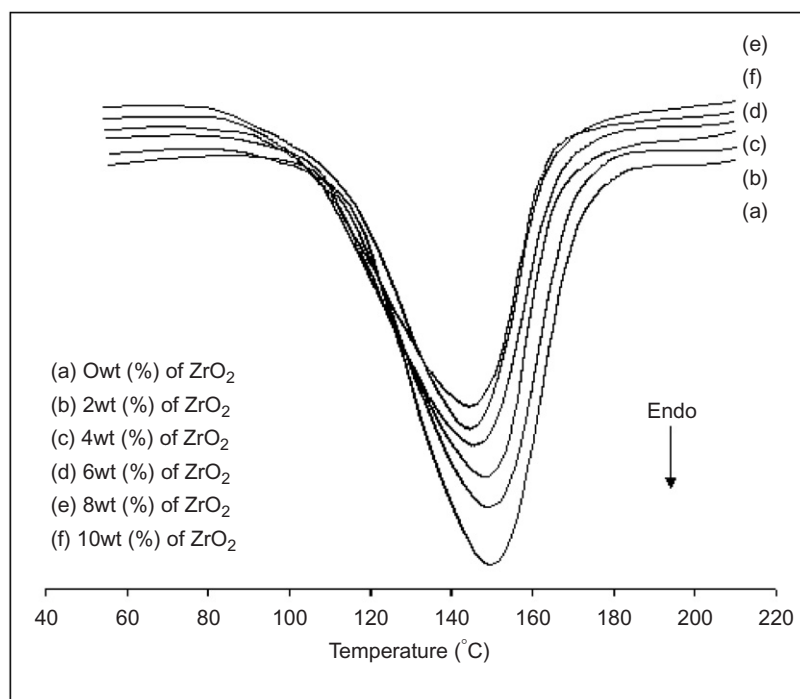


Fig. 3. DSC curve of PVdF-co-HFP-ZrO₂-based NCPMs containing different wt (%) of ZrO₂ nanoparticles.

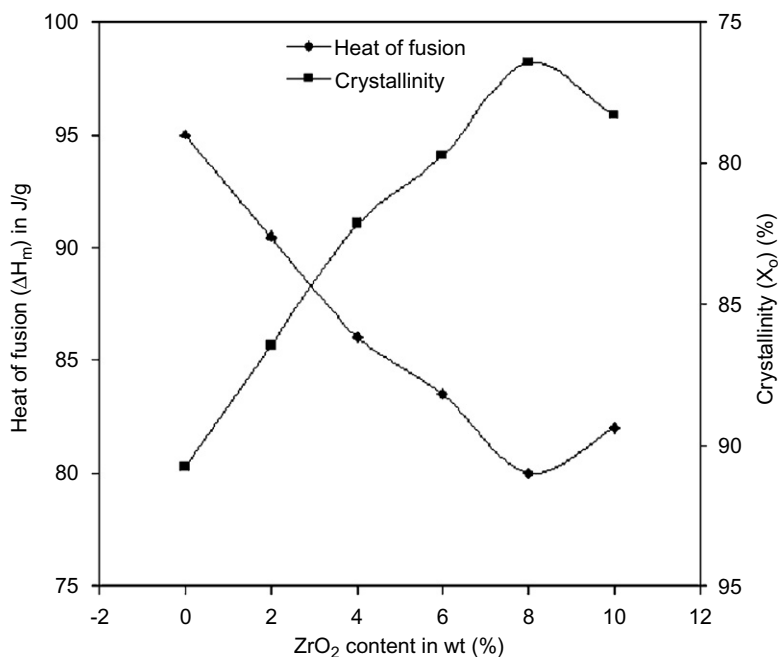


Fig. 4. Crystallinity and heat of fusion of PVdF-co-HFP-ZrO₂-based NCPMs containing different wt (%) of ZrO₂ nanoparticles.

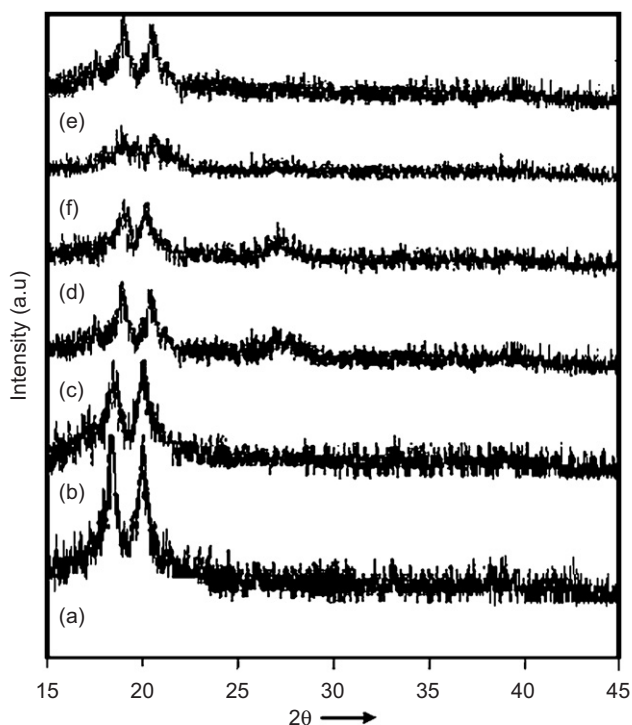


Fig. 5. XRD patterns of PVdF-co-HFP-based NCPMs containing different wt(%) of ZrO₂ nanoparticles. (a) 0 wt (%) of ZrO₂, (b) 2 wt (%) of ZrO₂ (c) 4 wt (%) of ZrO₂ (d) 6 wt (%) of ZrO₂ (e) 8 wt (%) of ZrO₂ (f) 10 wt (%) of ZrO₂.

3.3. XRD analysis of NCPMs

X-ray diffraction patterns of PVdF-co-HFP-ZrO₂-based NCPMs obtained from different wt(%) of ZrO₂ nanoparticles [0 wt(%), 2 wt(%), 4 wt(%), 6 wt(%), 8 wt (%) and

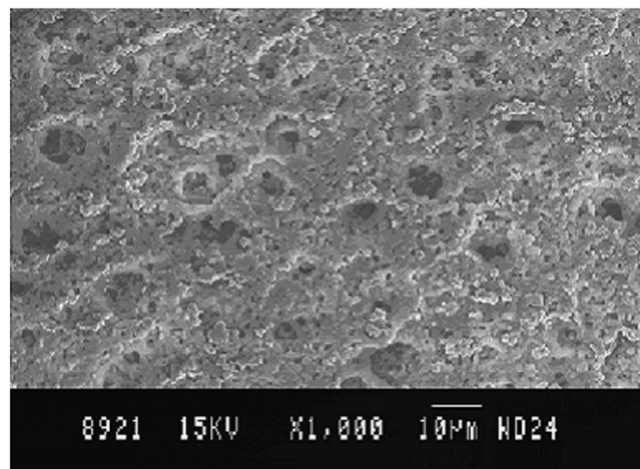


Fig. 6. SEM photograph of NCPM containing 8 wt (%) of ZrO₂ content.

10 wt(%) are shown in Fig. 5 (a)–(f). From the XRD patterns, the following distinct features were observed:

1. The decrease in relative intensity of the apparent peaks were observed with increase in ZrO₂ content upto 8 wt% [Fig. 5 (a)–(e)]. This is because decrease in crystallinity of PVdF-co-HFP matrix created the space charge layer at the filler–polymer interface to assist the transport of ions and ZrO₂ may influence the recrystallization kinetics of PVdF-co-HFP chain to promote localized amorphous region which is in good agreement with DSC results.
2. Further increase in concentration of ZrO₂ [10 wt(%)] increases the relative intensity of apparent peaks. It may be attributed to the phase separation of zirconia from the PVdF-co-HFP matrix because the aggregated

nanoparticles are not consistent with the polymer matrix [Fig. 5(f)].

3.4. SEM analysis of NCPMs

Fig. 6 shows the SEM photograph of nano-composite polymer membrane (NCPM) of high ionic conductivity system. It can be seen from the figure that the ZrO_2 nanoparticles are distributed uniformly in the polymer

matrix and some tiny pores existed between the filler–polymer interfaces. It may be suggested that the liquid electrolyte is present both in pores and the PVdF-co-HFP polymer matrix which may provide the fast ion transport.

3.5. AC-impedance analysis of NCPMs

The particle size and the mass of ceramic filler in the polymer matrix plays an important role in ionic

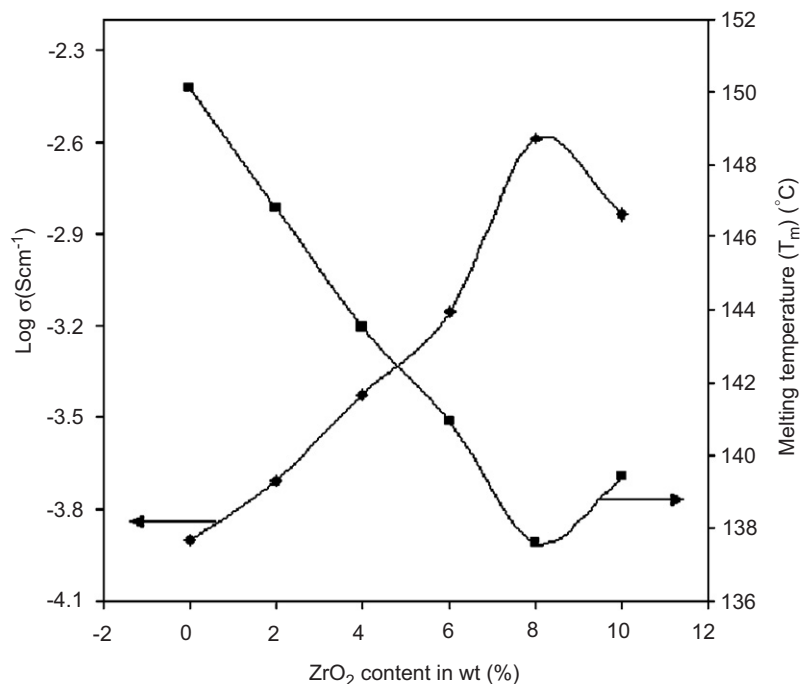


Fig. 7. The relationship between T_m and ionic conductivity of NCPM with respect to ZrO_2 content.

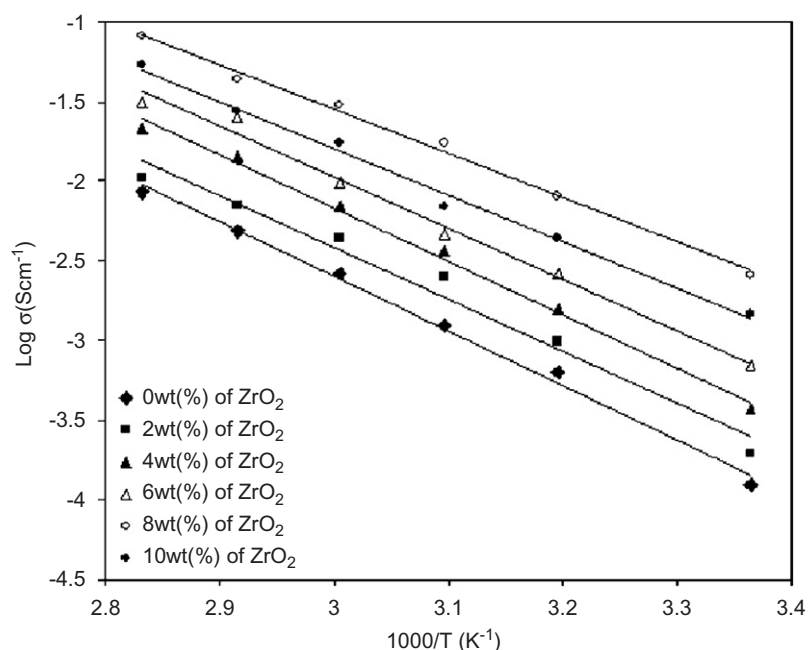


Fig. 8. Temperature depends on ionic conductivity of NCPM containing different wt (%) of ZrO_2 nanoparticles.

conductivity. Fig. 7 shows the ionic conductivity of different wt (%) of inclusion of ZrO_2 nanoparticles in the PVdF-co-HFP matrix at room temperature. It can be observed from Fig. 7 that the ionic conductivity increases with increase in ZrO_2 content up to 8 wt(%) of the PVdF-co-HFP matrix which bring localized amorphous regions and ceramic–salt interactions. Hence, ionic conductivity of NCPEM increases [20]. Beyond this concentration, ionic conductivity decreases. It may be probably because increasing the crystallinity and viscosity of PVdF-co-HFP matrix may trap the ion mobility.

The relationship between T_m and ionic conductivity with respect to ZrO_2 content is shown in Fig. 7. The rise value of T_m with inclusion of ZrO_2 over 8 wt(%) may increase the crystallization site or cause a molecular interaction between the polymer chains which leads to lower mobility. On the basis of the characterization results, it is feasible to postulate a model to describe the Lewis acid–base interaction in PVdF-co-HFP- ZrO_2 - $LiClO_4$

composite. Such interaction prevents PVdF-co-HFP molecules from crystallinity and also releases more free Li^+ ions. Besides, the ClO_4^- anions are also bound to the Lewis acid sites (O-vacancies) through coordination, which separates the $Li^+ClO_4^-$ pairs. These two modes of coordination produce more dissociated Li^+ ions as charge carrier and more amorphous region for the carrier to transfer. Hence, ionic conductivity of the NCPEMs was increased.

Fig. 8 shows the ionic conductivity of PVdF-co-HFP- ZrO_2 matrix as a function of different wt (%) of ZrO_2 content at various temperatures in the range of 298 to 353 K. The 8 wt(%) ZrO_2 incorporation of PVdF-co-HFP matrix shows relatively high ionic conductivity over a wide temperature range even at a lower temperature. It may be due to increasing the dissociation of lithium salt resulting in the enhancement of conductivity. But at higher concentrations of ZrO_2 [10 wt(%)] will build up a continuous non-conductive phase and hence this

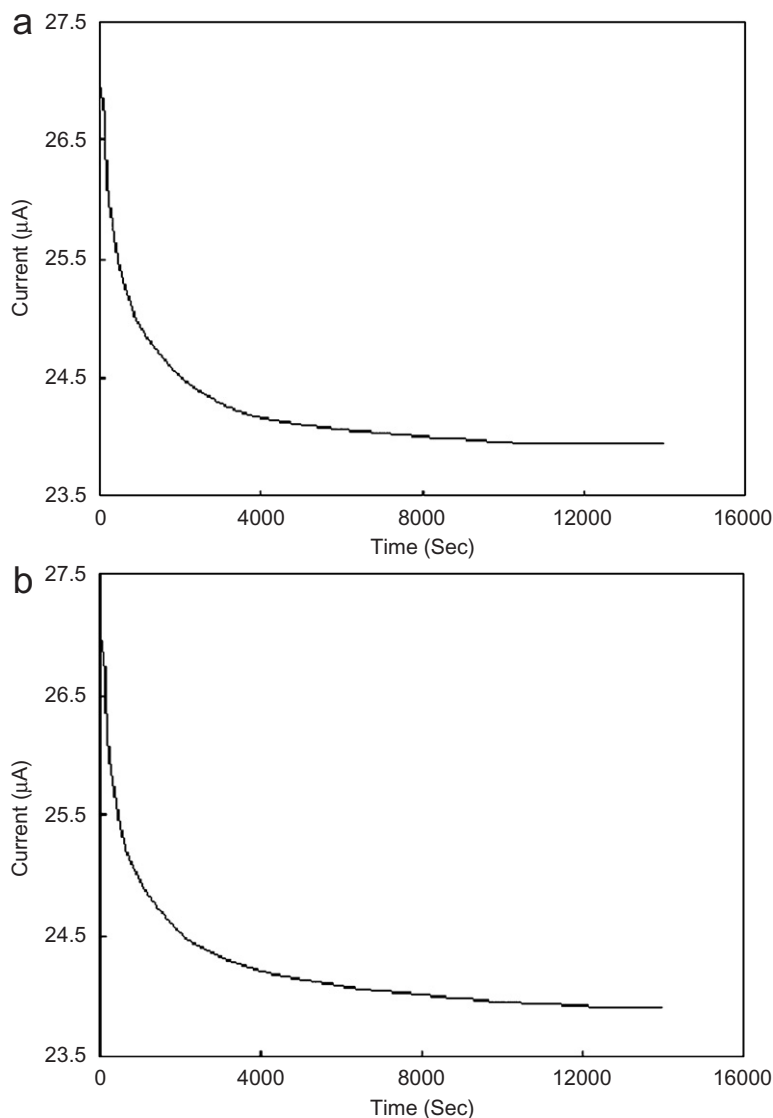


Fig. 9. DC-polarization curve of PVdF-co-HFP-based (a) GPE and (b) NCPEM of high ionic conductivity system.

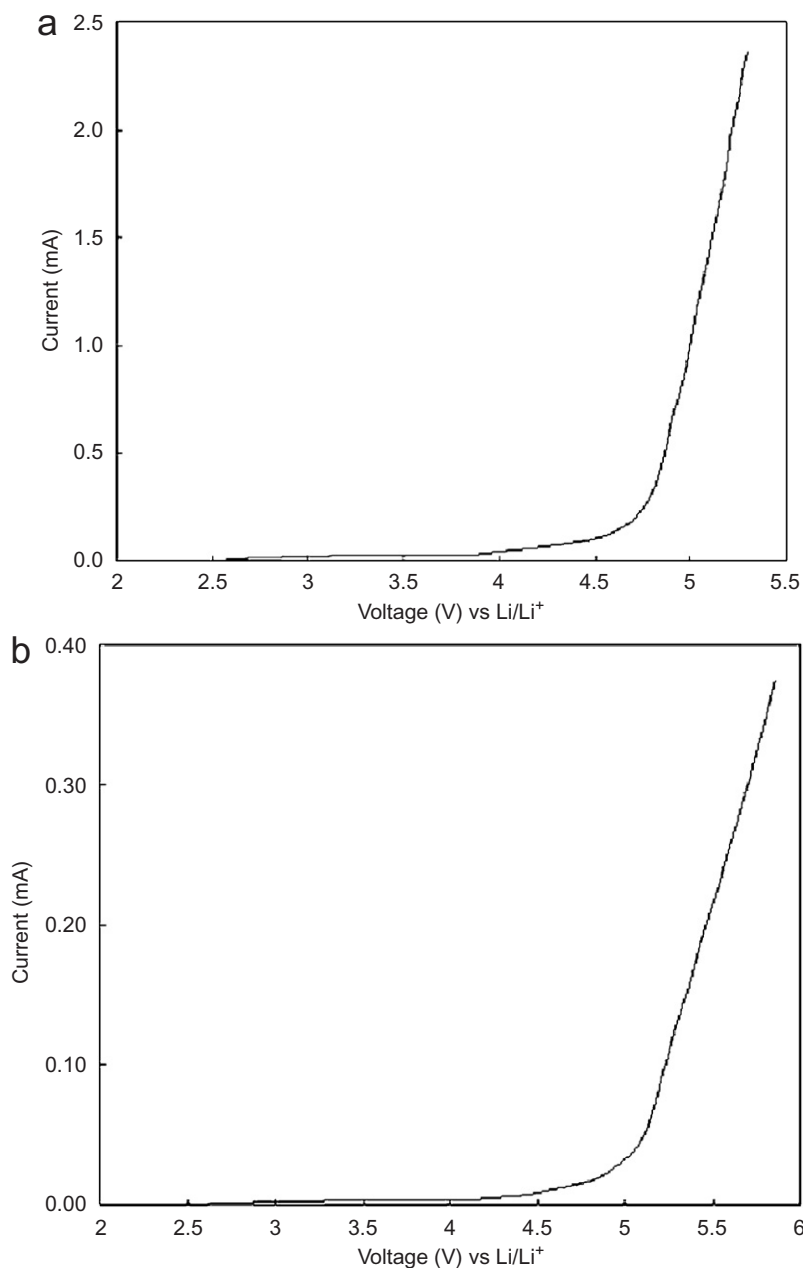


Fig. 10. LSV curve of PVdF-co-HFP-based (a) GPE and (b) NCPem of high ionic conductivity system.

electrically inert filler would block up lithium-ion transport resulting in an increase of total resistance of the NCPems.

3.6. Transference number

The transference number of PVdF-co-HFP-based gel polymer electrolyte (GPE) and NCPem of high ionic conductivity system was found out by means of chronoamperometric technique as shown in Fig. 9(a) and (b) and

its impedance measurements were obtained before and after DC-polarization measurements with an applied potential difference of 10 mV/s. It can be seen from the Fig. 9(b) that the initial current value (I_0) is 26.95 μ A and steady-state value (I_s) is 23.94 μ A within about 3.21 h and its corresponding AC-impedance values such as initial resistance of interface (R_i^0) and steady-state resistance of interface (R_i^s) are 218.34 and 300.21 Ω , respectively, which gives the transference number (t_+) ca. 0.729. Fig. 9(a)

shows that the initial current value (I_0) is $26.89\ \mu\text{A}$ and steady-state value (I_s) is $23.07\ \mu\text{A}$ within about 4.20 h and its corresponding AC-impedance values such as initial resistance of interface (R_i^0) and steady-state resistance of interface (R_i^s) are 264.56 and $460.27\ \Omega$, respectively, which gives the transference number (t_+) ca. 0.574 and also this relaxation time of nano-composite polymer electrolyte membrane (NCPem) is much faster than the GPE. Theoretically, this phenomenon implies that the ionic mobility of NCPem is more facile than the conventional gel polymer electrolyte. Hence, the inclusion of ZrO_2 onto the PVdF-co-HFP polymer matrix that provides more liquid pathway is probably a positive factor leading to superior ionic transport as well.

3.7. Electrochemical stability

Fig. 10(a) and (b) shows the current–voltage response obtained for both PVdF-co-HFP-based GPE and NCPem of high ionic conductivity system. It can be observed from the voltammograms that the anodic decomposition limit of the polymer electrolyte can be considered as the voltage at which the current flows through the cell. The observed anodic limit of NCPem is about $5.0\ \text{V}$ vs Li/Li^+ and was higher than that of GPE (about $4.7\ \text{V}$ vs Li/Li^+). It confirms that the inclusion of ZrO_2 onto PVdF-co-HFP polymer matrix has a beneficial effect to widen the electrochemical stability window.

4. Conclusions

A nano-composite polymer electrolyte membrane (NCPem) based on PVdF-co-HFP with ZrO_2 nanoparticles have been developed and examined. The dependence of ionic conductivity with respect to ZrO_2 content onto PVdF-co-HFP matrix revealed that crystallinity and viscosity are the two major factors that influence the ion mobilities. The lithium transference number of PVdF-co-HFP- ZrO_2 -based NCPem of high ionic con-

ductivity system was found to be 0.729. The LSV study revealed that the NCPem is electrochemically stable up to $5.0\ \text{V}$ vs Li/Li^+ . From the results, it is proposed that, the PVdF-co-HFP- ZrO_2 -based NCPems is a new promising candidate for high voltage lithium-ion batteries.

Acknowledgements

The authors gratefully acknowledge the DST, New Delhi for the financial support.

References

- [1] M. Armand, *Solid State Ionics* 60 (1994) 309.
- [2] E. Quartarone, P. Mustarilli, A. Magistris, *Solid State Ionics* 110 (1998) 1.
- [3] F. Croce, G.B. Appetecchi, L. Persi, B. Scrosati, *Nature* 394 (1998) 456.
- [4] L.Z. Fan, C.W. Nan, Z.M. Dang, *Electrochim. Acta* 47 (2002) 3541.
- [5] B. Scrosati, F. Croce, L. Persi, *J. Electrochem. Soc.* 5 (2000) 1718.
- [6] G.B. Appetecchi, F. Croce, L. Persi, F. Ronci, B. Scrosati, *Electrochim. Acta* 45 (2000) 1481.
- [7] W. Wieczorek, J.R. Stevens, Z. Florjanczk, *Solid State Ionics* 85 (1996) 76.
- [8] F. Croce, R. Curini, A. Martinello, L. Persi, F. Ronci, B. Scrosati, R. Caminiti, *J. Phys. Chem.* 103 (1999) 10632.
- [9] Seshumani Vorrey, Dale Teeters, *Electrochim. Acta* 48 (2003) 2137.
- [10] C.W. Nan, *Prog. Mater. Sci.* 37 (1993) 1.
- [11] W. Wieczorek, D. Raducha, A. Zalewska, *J. Phys. Chem. B* 102 (1998) 8725.
- [12] W. Wieczorek, A. Zalewska, D. Raducha, Z. Florjanczyk, J.R. Stevens, *Macromolecules* 29 (1996) 143.
- [13] Binod Kumar, L. Scanlon, R. Manson, R. Higgins, R. Baldwin, *Electrochim. Acta* 46 (2001) 1515.
- [14] G. Sandi, K.A. Carrado, H. Joachin, Jai prakash, *J. Power Sources* 119–121 (2003) 492.
- [15] Z. Li, G. Su, X. Wang, D. Gaw, *Solid State Ionics* 176 (2005) 1903.
- [16] P.G. Bruce, C.A. Vencent, *J. Electroanal. Chem.* 225 (1987) 1.
- [17] S. Benfer, E. Knozinger, *J. Mater. Chem.* 9 (1999) 1203.
- [18] H.M. Xiong, X. Zhao, J.S. Chen, *J. Phys. Chem. B* 105 (2001) 10169.
- [19] B.J. Ash, L.S. Schadler, R.W. Siegel, *Matter. Lett.* 55 (2002) 83.
- [20] B. Kumar, S.J. Rodrigues, *J. Electrochem. Soc.* 148 (2001) A1336.